

# Upper Limit Set by Causality on the Rotation and Mass of Uniformly Rotating Relativistic Stars

Scott Koranda

Department of Physics, Case Western Reserve University,  
10900 Euclid Avenue, Cleveland, OH 44106-7079

Nikolaos Stergioulas

Department of Physics, University of Wisconsin-Milwaukee,  
P.O. Box 413, Milwaukee, WI 53201

John L. Friedman

Department of Physics, University of Wisconsin-Milwaukee,  
P.O. Box 413, Milwaukee, WI 53201

November 26, 2024

## Abstract

Causality alone suffices to set a lower bound on the period of rotation of relativistic stars as a function of their maximum observed mass. That is, by assuming a one-parameter equation of state (EOS) that satisfies  $v_{\text{sound}} < c$  and that allows stars with masses as large as the largest observed neutron-star mass,  $M_{\text{sph}}^{\text{max}}$ , we find  $P[\text{ms}] > 0.282 + 0.196 \left( M_{\text{sph}}^{\text{max}} / M_{\odot} - 1.442 \right)$ . The limit does *not* assume that

the EOS agrees with a known low-density form for ordinary matter, but if one adds that assumption, the minimum period is raised by a few percent. Thus the *current* minimum period of uniformly rotating stars, set by causality, is 0.28ms (0.29ms for stars with normal crust). The minimizing EOS yields models with a maximally soft exterior supported by a maximally stiff core. An analogous upper limit set by causality on the maximum mass of rotating neutron stars requires a low-density match and the limit depends on the matching density,  $\epsilon_m$ . We recompute it, obtaining a slightly revised value,

$$M_{rot}^{max} \simeq 6.1 (2 \times 10^{14} \text{ g/cm}^3 / \epsilon_m)^{1/2} M_\odot.$$

# 1 INTRODUCTION

The upper limit set by gravity on the rotation of neutron stars is sensitive to the equation of state (EOS) above nuclear density, and the current large uncertainty in the EOS implies a large uncertainty in the maximum rate of rotation. One can, however, find an upper limit on rotation which is independent of the EOS. This limit is set by causality together with the requirement that the EOS allows stars with masses as large as the largest observed neutron-star mass.

Glendenning (1992) first estimated this causally limited period for gravitationally bound stars. He considered a flexible two-parameter, gamma-law ansatz for the EOS at high energy density; by varying the two parameters, he found equations of state (EOSs) which appeared to minimize the period as a function of the maximum nonrotating (or spherical) mass  $M_{sph}^{max}$  allowed by the EOS. Our work improves upon his estimate in several ways. First, where Glendenning used an empirical formula to estimate the minimum period from a set of nonrotating models, we construct models using a code that constructs rapidly rotating relativistic stars. Second, our numerical investigation singles out a simple analytic form for the EOS which minimizes the period for a given  $M_{sph}^{max}$ . This minimum-period EOS has a simple physical interpretation; it allows the most centrally condensed star while still supporting a mass  $M_{sph}^{max}$ . Specifically, we find that if  $M_{sph}^{max} = 1.442 M_{\odot}$  (currently the largest accurately measured mass of neutron stars (Taylor &

Weisberg 1989), the minimum period allowed is 0.28ms. This minimum period is about 13 % less than that estimated by Glendenning (1992). Third, we emphasize that there exists an upper limit on rotation set only by causality, which requires no matching to a low density EOS. Finally, we find an exact scaling between the minimum period  $P_{min}$  and  $M_{sph}^{max}$ . The scaling is due to the specific form of the minimum-period EOS, and implies that the central energy densities, masses, and radii of the maximum-mass spherical (and maximum-mass rotating) stars scale between different minimum-period EOSs.

The maximum mass of gravitationally bound stars set by causality is, in contrast, quite sensitive to the matching density (Hartle & Sabbadini 1977) (the initial Rhoades and Ruffini (1974) limit was computed for a particular choice of matching density). For rotating neutron stars, the maximum mass set by causality was first obtained by Friedman and Ipser (1987). This maximum mass has not, however, however been recomputed since recent improvements in relativistic, rotating star codes, and we do so here. Using the FPS EOS (Pandharipande & Ravenhall 1989) at low density, we find  $M_{max} = 6.1M_{\odot}(\epsilon_m/2 \times 10^{14}g/cm^3)^{-1/2}$ , where  $\epsilon_m$  is the matching energy density.

## 2 ASSUPMTIONS FOR THE EQUATION OF STATE

For number densities  $n \leq 0.1 \text{ fm}^{-3}$  (slightly less than nuclear saturation density) the FPS EOS (Pandharipande & Ravenhall 1989) is expected to describe normal matter with reasonable accuracy (Ravenhall 1995). Above this density, however, current observations are compatible with a variety of proposed equations of state that span a large range of compressibilities and predict correspondingly different minimum periods. One can, however, use causality to set a lower limit on the rotation period of stable relativistic stars that is independent of the high density EOS. More precisely, we assume:

- (0) *A relativistic star is described as a self-gravitating, uniformly rotating perfect fluid with a one-parameter EOS.*

Cold neutron stars satisfy this assumption to high accuracy (Friedman & Ipser 1992).

- (1)  $v_{sound} \equiv \sqrt{dp/d\epsilon} \leq 1.$

Here  $v_{sound}$  is the phase velocity of sound waves,  $p$  the pressure, and  $\epsilon$  the energy density of the stellar perfect fluid matter. Relativistic fluids are governed by hyperbolic equations whose characteristics lie outside the light cone (and thus their initial value formulation violates causality) if  $v_{sound} > 1$  (here and throughout the paper we have set  $c = 1$ ) (Geroch & Lindblom 1991). That is, if both the equilibrium

star and its small oscillations are described by a one-parameter EOS, then assumption (1) is implied by causality.

These two assumptions alone yield an upper limit on rotation as a function of the maximum observed mass of a relativistic star. Only a slightly more stringent limit is obtained if one makes the further assumption:

- (2) *The EOS is known (matches FPS) at low density.*

Relativistic stars with normal crusts are thought to be accurately described by the FPS EOS up to number densities  $n \approx 0.1 \text{ fm}^{-3}$ . We adopt  $n_m = 0.1 \text{ fm}^{-3}$  as a conservative value for the number density  $n_m$  at which the EOS at high density must match the FPS EOS for low densities.

Below we examine limits on the rotation of stable equilibrium models corresponding first to assumptions (0) and (1) only, and then to assumptions (0)-(2); as noted, we find that the additional assumption of a match to the known low-density equation of state has a small effect on the minimum period computed using (0) and (1) only.

### 3 EQUATION OF STATE YIELDING THE UPPER LIMIT ON ROTATION

A uniformly rotating, gravitationally bound star rotates with a period greater than or equal to its Kepler period. The Kepler period is the period of a free

particle in circular orbit at the star's equator. A soft EOS yields stellar models with dense central cores, large binding energies, and thus smaller Kepler periods than models built from stiff EOSs. Soft EOSs, however, cannot support massive stars. This suggests that models with minimum periods arise from EOSs which are stiff at high density, allowing stiff cores to support against collapse, but soft at low density, allowing small radii and thus fast rotation. Our numerical results are consistent with this expectation, and strongly suggest a simple form for the EOS yielding minimum period stars and satisfying the assumptions listed in section 2. We distinguish the two instances where the EOS does or does not match smoothly to the FPS EOS at low density and satisfy assumption (2) above.

### 3.1 Minimum-Period EOS

Considering only assumptions (0) and (1), so that the EOS is constrained only by causality, the EOS yielding the minimum period stars for a given maximum spherical star mass  $M_{sph}^{max}$  is divided into two regions. Above a density  $\epsilon_C$  the EOS is maximally stiff with  $dp/d\epsilon = 1$ , while for  $\epsilon \leq \epsilon_C$  the EOS is maximally soft with vanishing pressure  $p = 0$ :

$$p(\epsilon) = \begin{cases} 0 & \epsilon \leq \epsilon_C, \\ \epsilon - \epsilon_C & \epsilon \geq \epsilon_C. \end{cases} \quad (1)$$

This EOS is depicted in Figure 1. It gives a stringent upper limit set by causality on the rotation of uniformly rotating, gravitationally bound stars, independent of any specific knowledge about the EOS for the matter com-

posing the star. The energy density  $\epsilon_C$  is the single free parameter of this minimum-period EOS. By choosing  $\epsilon_C$  one selects the maximum spherical star mass  $M_{sph}^{max}$  that the minimum-period EOS allows. Further, a one to one correspondence exists between  $\epsilon_C$  and other characteristics of the minimum-period EOS, such as the maximum mass of rotating stars.

### 3.2 Minimum-Period EOS with FPS Low Density EOS

Considering assumptions (0), (1) and (2) above, so that the EOS matches the FPS EOS at low density, the minimum-period EOS is divided into three regions. Above a density  $\epsilon_C$  the minimum-period EOS is maximally stiff with  $dp/d\epsilon = 1$ . Between the matching density to the FPS EOS  $\epsilon_m$  and  $\epsilon_C$  the EOS is maximally soft with  $dp/d\epsilon = 0$ . Below  $\epsilon_m$  the EOS is given by the FPS EOS. Explicitly,

$$p(\epsilon) = \begin{cases} p_{\text{FPS}}(\epsilon) & \epsilon \leq \epsilon_m, \\ p_m & \epsilon_m \leq \epsilon \leq \epsilon_C, \\ p_m + \epsilon - \epsilon_C & \epsilon \geq \epsilon_C. \end{cases} \quad (2)$$

This EOS is also depicted in Figure 1. The maximally soft, constant pressure region corresponds to a first-order phase transition for a single component system. For a fixed low density EOS and matching energy density  $\epsilon_m$ , the causal limit energy density  $\epsilon_C$  parameterizes the class of minimum-period EOSs. Again, by choosing  $\epsilon_C$  one selects the maximum spherical star mass  $M_{sph}^{max}$  that the minimum-period EOS allows, and a one to one correspondence exists between  $\epsilon_C$  and other characteristics of the minimum-period EOS.

Figure 2 shows the minimum-period EOS (1) yielding a maximum mass spherical star with  $M_{sph}^{max} = 1.442 M_{\odot}$ . The energy density at which the EOS changes from zero pressure to  $dp/d\epsilon = 1$  is  $\epsilon_C = 2.156 \times 10^{15} g/cm^3$ , and the central energy density of the minimum-period star is  $4.778 \times 10^{15} g/cm^3$ . Also shown in Figure 2 is the minimum-period EOS (2) which matches to the FPS EOS at  $n_m = 0.1 fm^{-3}$  and yields a maximum mass spherical star with  $M_{sph}^{max} = 1.442 M_{\odot}$ . For this EOS  $\epsilon_C = 2.157 \times 10^{15} g/cm^3$  and the central energy density of the minimum-period star is  $5.274 \times 10^{15} g/cm^3$ . The numerical work leading to the EOSs (1) and (2) is outlined in section 4.

Figure 3 shows the minimum period  $P_{min}$  of gravitationally bound stars as a function of the maximum allowed mass of nonrotating stars  $M_{sph}^{max}$ . The lower curve (which is a straight line) corresponds to the minimum-period EOS (1) satisfying assumptions (0) and (1), while the upper curve corresponds to the minimum-period EOS (2) matched to the FPS EOS at  $n_m = 0.1 fm^{-3}$ .

The minimum-period EOS (1) yields stars entirely at the causal limit with a nonzero surface energy density  $\epsilon_C$ . This surface energy density  $\epsilon_C$  is the only free parameter and the only dimensionful parameter. The family of maximally rotating equilibrium stars yielded by the minimum-period EOS (1) with different  $\epsilon_C$  are characterized by this one dimensionful parameter; it follows that all properties of the maximally rotating stars scale according to their dimensions in gravitational units (with  $c = G = 1$ ),  $[\epsilon] = [M^{-2}]$ ,  $[P] = [M] = [R]$ . Thus, the following relations hold between different maximally

rotating stars computed from minimum-period EOSs with different  $\epsilon_C$ :

$$P \propto M_{sph}^{max} \propto R_{sph}^{max}, \quad (3)$$

$$\epsilon_{sph}^{max} \propto \frac{1}{(M_{sph}^{max})^2}, \quad (4)$$

$$M_{rot}^{max} \propto M_{sph}^{max}, \quad (5)$$

$$R_{rot}^{max} \propto R_{sph}^{max}, \quad (6)$$

$$\epsilon_{rot}^{max} \propto \epsilon_{sph}^{max}, \quad (7)$$

where  $R$  is the equatorial radius. Numerically, we find the linear relation

$$P_{\min}[ms] = 0.200 M_{sph}^{max} / M_{\odot}, \text{ or}$$

$$\frac{P_{\min}}{ms} = 0.288 + 0.200 \left( \frac{M_{sph}^{max}}{M_{\odot}} - 1.442 \right). \quad (8)$$

(Note, however, that we have only considered the period of the maximum-mass rotating model. In general the maximum-mass model is distinct from the minimum-period model, but the difference in the period between the two models is small. See section 6.)

The upper curve in Figure 3 corresponds to EOSs (2) which match the FPS EOS at low density. This curve is almost linear, since the matching number density  $n_m = 0.1 \text{ fm}^{-3}$  is low enough that the causal limit region of the EOS dominates the bulk properties of the star. That is, a minimum-period star with a low matching density mimics a star *entirely* at the causal limit and having a nonzero surface energy equal to  $\epsilon_C$ . Hence the scaling relations above are nearly exact for minimum-period stars with low matching

density. Numerically we find for the EOSs (2)

$$\frac{P_{\min}}{ms} = 0.295 + 0.203 \left( \frac{M_{sph}^{\max}}{M_{\odot}} - 1.442 \right), \quad (9)$$

which is linear to an accuracy better than 0.5 %. For  $M_{sph}^{\max} = 1.442 M_{\odot}$  the minimum period is 0.29 ms. The above formulae allow one to calculate without intensive numerical computations the absolute minimum period if and when new observations revise the current  $M_{sph}^{\max} = 1.442 M_{\odot}$  limit.

## 4 NUMERICAL EVIDENCE IN SUPPORT OF THE MINIMUM-PERIOD EOS

As noted above, our numerical results are consistent with the expectation that the EOSs yielding the minimum-period stars are maximally stiff at high density and maximally soft at low density. Below we present the numerical evidence supporting our claim that the EOSs (1) and (2) yield the maximum rotating stars, and detail how we searched the space of EOSs to find the minimum-period EOS (2).

### 4.1 Perturbations to the Minimum-Period EOS

Evidence that the minimum-period EOS (2) yields the fastest rotating stars is shown in Figure 4. Each point in Figure 4 represents an EOS obtained by making a “small” perturbation to the minimum-period EOS (2), and lies *above* the solid curve obtained from the minimum-period EOS. For any particular  $M_{sph}^{\max}$  the perturbed EOSs yield maximally rotating stars which

rotate *slower* than the maximally rotating stars yielded by the minimum-period EOSs.

We considered three different types of perturbations to the minimum-period EOS. The first type of perturbed EOS considered is obtained from the minimum-period EOS by adding a “step function” to the minimum-period EOS :

$$p(\epsilon) = \begin{cases} p_{\text{FPS}}(\epsilon) & \epsilon \leq \epsilon_m, \\ p_m & \epsilon_m \leq \epsilon \leq \epsilon_1, \\ p_m + \epsilon - \epsilon_1 & \epsilon_1 \leq \epsilon \leq \epsilon_2, \\ p_m + \epsilon_2 - \epsilon_1 & \epsilon_2 \leq \epsilon \leq \epsilon_C, \\ p_m + \epsilon_2 - \epsilon_1 + \epsilon - \epsilon_C & \epsilon \geq \epsilon_C. \end{cases} \quad (10)$$

By varying  $\epsilon_1$  and  $\epsilon_2$ , as well as  $\epsilon_C$ , we sampled a large number of perturbed minimum-period EOSs. For  $\epsilon_2 - \epsilon_1$  small, the minimum period for a given  $M_{\text{sph}}^{\text{max}}$  allowed by the perturbed EOS is slightly *larger* than that yielded by the minimum-period EOS (2). The minimum periods obtained using the “step function” perturbations are indicated by the open squares in Figure 4. For  $\epsilon_2 - \epsilon_1$  large, the minimum periods yielded by the perturbed EOS are much larger and are not shown in Figure 4. Thus a small perturbation away from the minimum-period EOS (2) *increases* the minimum period for a given  $M_{\text{sph}}^{\text{max}}$ .

The second type of perturbation to the minimum-period EOS we considered is obtained by decreasing the slope  $dp/d\epsilon$  away from unity for the causal

$(\epsilon \geq \epsilon_C)$  part of the minimum-period EOS. The filled triangles in Figure 4 indicate the minimum periods obtained by perturbing the minimum-period EOS in this way. Again, the minimum period increases when the minimum-period EOS (2) is perturbed. The third type of perturbation we considered is obtained by increasing the slope  $dp/d\epsilon$  away from zero for the constant pressure or  $\epsilon_m \leq \epsilon \leq \epsilon_C$  part of the minimum-period EOS. For  $\epsilon \geq \epsilon_C$  the perturbed EOS again is at the causal limit with  $dp/d\epsilon = 1$ . The crosses in Figure 4 indicate the minimum periods obtained by perturbing the minimum-period EOS in this way, and again the minimum period increases when the minimum period EOS (2) is perturbed.

We have sampled a large number of perturbed minimum-period EOSs which satisfy assumptions (0), (1), and (2) of section 2, and have found that the minimum period allowed by a perturbed EOS for a given  $M_{sph}^{max}$  is always greater than the minimum period yielded by the minimum-period EOS (2). These results, taken together with results obtained from a two parameter ansatz EOS described in the next section, strongly suggest that the minimum-period EOS (2) is the EOS which provides the upper limit set by causality for the rotation of gravitationally bound stars.

## 4.2 Ansatz for Searching the Space of Equations of State

To search the restricted space of EOSs which satisfy the assumptions in section 2, and to determine the class of EOSs which yield the minimum

period stars, we follow Glendenning (1992) and adopt a simple ansatz for the EOS. For low number density, the energy density and pressure are

$$\epsilon(n) = \epsilon_{\text{FPS}}, \quad (11)$$

$$p(n) = p_{\text{FPS}}, \quad (12)$$

where  $\epsilon_{\text{FPS}}$  and  $p_{\text{FPS}}$  correspond to the FPS EOS. Above some number density  $n_m$ , where the FPS EOS is suspect, the energy density and pressure are

$$\epsilon(n) = p_m \left\{ \frac{\kappa}{\gamma-1} \left[ \left( \frac{n}{n_m} \right)^\gamma - \frac{n}{n_m} \right] + \frac{n}{n_m} \frac{\epsilon_m}{p_m} + \left( 1 - \frac{n}{n_m} \right) (\kappa - 1) \right\}, \quad (13)$$

$$p(n) = p_m \left\{ \kappa \left[ \left( \frac{n}{n_m} \right)^\gamma \right] + 1 \right\}, \quad (14)$$

where  $\epsilon_m$  and  $p_m$  are the energy density and pressure at the matching number density  $n_m$ , which is typically  $0.1 \text{ fm}^{-3}$ . The two dimensionless parameters  $\kappa$  and  $\gamma$  parameterize the restricted EOS space. Assumptions (0) and (1) of section 2 require

$$\gamma > 1, \quad (15)$$

$$\kappa > 0, \quad (16)$$

$$\kappa\gamma \leq \frac{\epsilon_m}{p_m} + 1. \quad (17)$$

Given  $\kappa$  and  $\gamma$ , we use the parameterized form (13) and (14) for densities greater than the matching density  $n_m$ , but only if the EOS remains causal. If above some density  $n_C$  the equation of state reaches the causal limit, so that  $\frac{dp}{d\epsilon} > 1$ , then for  $n > n_C$  the parameterized EOS is matched to an EOS which is always at the causal limit. In this instance the energy density and

pressure above  $n_C$  are

$$\epsilon(n) = \epsilon_C - p_C + p(n), \quad (18)$$

$$p(n) = \frac{1}{2} \left\{ p_C - \epsilon_C + (p_C + \epsilon_C) \left( \frac{n}{n_C} \right)^2 \right\}, \quad (19)$$

where  $\epsilon_C$  and  $p_C$  are the energy density (13) and pressure (14) evaluated at  $n_C$ . Note that the parameterization of pressure as a function of number density is arbitrary, since (18) assures that  $\frac{dp}{d\epsilon} = 1$ . If  $\kappa$  and  $\gamma$  are chosen so that the EOS remains causal then the parameterized form is used for all densities  $n \geq n_m$ . Combining the different expressions for the different ranges of number density the EOS is

$$\epsilon(n) = \begin{cases} \epsilon_{\text{FPS}}(n) & n \leq n_m, \\ p_m \left\{ \frac{\kappa}{\gamma-1} \left[ \left( \frac{n}{n_m} \right)^\gamma - \frac{n}{n_m} \right] + \frac{n}{n_m} \frac{\epsilon_m}{p_m} + \left( 1 - \frac{n}{n_m} \right) (\kappa - 1) \right\} & n_m \leq n \leq n_C, \\ \epsilon_C - p_C + p(n) & n \geq n_C, \end{cases} \quad (20)$$

$$p(n) = \begin{cases} p_{\text{FPS}}(n) & n \leq n_m, \\ p_m \left\{ \kappa \left[ \left( \frac{n}{n_m} \right)^\gamma \right] + 1 \right\} & n_m \leq n \leq n_C, \\ \frac{1}{2} \left\{ p_C - \epsilon_C + (p_C + \epsilon_C) \left( \frac{n}{n_C} \right)^2 \right\} & n \geq n_C, \end{cases} \quad (21)$$

where the  $n \geq n_C$  case applies only if  $n_C$  exists and is finite. Note that the EOS is continuous, although its first derivative may be discontinuous at  $n_m$ . We do not include a separate expression for the possibility of a  $p = \text{constant}$ , one-component first-order phase transition region, since this may be attained in the limit as  $\kappa \rightarrow 0$ . One may search the restricted EOS space using (20) and (21) by varying the parameters  $\kappa$  and  $\gamma$ .

The two-parameter EOS (20) and (21) does not span the entire restricted EOS space. Still, as Figure 5 shows, it is quite flexible, and spans a representative subspace which includes both soft and stiff EOSs. This two-parameter family of EOSs proved sufficient to identify the class of EOSs yielding the minimum-period stars.

### 4.3 Searching for the Minimum-Period Star

We used a fully relativistic, numerical code to compute rapidly rotating models of compact stars and find the maximum-mass model for a given EOS. Stergioulas (Stergioulas & Friedman 1995) wrote the code following the Cook, Shapiro and Teukolsky (1994) implementation of the Komatsu, Eriguchi and Hachisu (1989) method. Koranda made changes which substantially improved the speed of the code.

Using the flexible ansatz (20) and (21), we have searched for the class of EOSs which yield the minimum-period stars. As mentioned in the introduction, we are interested in the minimum period as a function of  $M_{sph}^{max}$ , the mass of the maximum mass nonrotating (spherical) star. We first used (20) and (21) to search for EOSs yielding particular values of  $M_{sph}^{max}$ . Having determined the  $\kappa$  and  $\gamma$  parameters for those EOSs yielding a particular  $M_{sph}^{max}$ , we then searched amongst those EOSs for the one which yielded the rotating star with the minimum period  $P_{min}$ . Figure 6 shows the results of our search for  $M_{sph}^{max} = 1.442 M_{\odot}$ . Each point along the curve defines an EOS which yields a maximum mass spherical star of mass  $M_{sph}^{max} = 1.442 M_{\odot}$ . As one

moves along the curve towards smaller and smaller values of  $\kappa$ , *the minimum period allowed by the EOS continues to decrease and tends asymptotically to a minimum as  $\kappa \rightarrow 0$ .*

That the period tends only asymptotically to a minimum as  $\kappa \rightarrow 0$  can be understood by considering the EOSs sampled as one moves along the curve in Figure 6. The bottom plot of Figure 5 shows the EOSs sampled as one moves along the curve in Figure 6. As one moves to small  $\kappa$  the EOS is essentially unchanged, approaching the minimum period EOS (2) with constant pressure from  $p_m$  to  $p_C$ . In the limit as  $\kappa \rightarrow 0$  one obtains the minimum period EOS (2) and the minimum period is given by the upper curve in Figure 3. This is true for all reasonable  $M_{sph}^{max}$ .

## 5 DEPENDENCE ON MATCHING DENSITY

Our results are fairly insensitive to the matching density at which the minimum-period EOS (2) is matched to the FPS EOS for low densities. This is because the matching density is low compared to the central densities of the minimum-period stars, and as noted above, the causality limited region of the EOS determines the bulk properties of the minimum-period stars. Thus requiring that the star have a crust of normal matter and satisfy assumption (2) of section 2 increases the minimum period by less than 2.5% for a matching density of  $n_m = 0.1 \text{ fm}^{-3}$  and any  $M_{sph}^{max}$ . We further increased the matching density to  $n_m = 0.25 \text{ fm}^{-3}$  (well beyond where one trusts the

FPS EOS) and the minimum period again increased by less than 4.5 % for any  $M_{sph}^{max}$ . This is shown in Figure 7. Our current understanding of the low density EOS has a small effect on the minimum period determined only by the causality constraint (1) of section 2.

## 6 ACCURACY CHECK

The numerical code used to construct rapidly rotating, fully relativistic compact star models was checked for accuracy in an extensive comparison to other codes (Eriguchi et al. 1996). The agreement of the codes for physical quantities of specific models was 0.1 % to 0.01 % or better, depending on the stiffness of the EOS. Determining the maximum-mass model for a given EOS requires computing a large number of models until one computes a model within some tolerance of the true maximum mass and Kepler limit. Since the mass vs. central energy density curve is approximately flat near the maximum mass, we used a finely spaced grid and small tolerances (hence a large number of computed models) to determine the maximum-mass model for a given EOS.

Still, for a given EOS the maximum-mass model is in general distinct from the minimum-period model. The intersection of the Kepler limiting curve with the line of onset of axisymmetric instabilities in a mass vs. central energy density plot defines the minimum-period model (Stergioulas & Friedman 1995; Cook et al. 1994). The onset of axisymmetric instabilities is

defined by the relation

$$\left( \frac{\partial M}{\partial \epsilon_{central}} \right)_J = 0, \quad (22)$$

where  $J$  is angular momentum. The central energy density at the intersection may be higher or lower than the central energy density of the maximum-mass model. In general, however, the central energy density, mass, period and other characteristics of the minimum-period and maximum-mass models nearly coincide. We have confirmed that this is also true for the minimum-period EOSs (1) and (2). Figure 8 is a plot of mass vs. central energy density for sequences of models with constant angular momentum constructed using the minimum-period EOS (1) and yielding  $M_{sph}^{max} = 1.442M_\odot$ . Also shown is the Kepler limiting curve and the axisymmetric instability line. The maximum-mass model has a central energy density of  $4.9 \times 10^{15} g/cm^3$  and a period of 0.288 ms. The star having the maximum angular velocity for this equation of state has a central energy density of  $5.3 \times 10^{15} g/cm^3$  and a period of 0.282 ms, which is only 2% less than the period of the maximum-mass model. Computing the period of the maximum-mass model, rather than the true minimum-period model, saves a tremendous amount of computing time and introduces an error not larger than 2 %.

## 7 COMPARISON TO EARLIER WORK

Glendenning (1992) first estimated a causally limited period for gravitationally bound stars. Rather than numerically computing rapidly rotating models, he computed nonrotating models and estimated the minimum period for

a given EOS using the empirical formula

$$\frac{P_{min}}{ms} = 0.873 \left( \frac{M_{sph}^{max}}{M_{\odot}} \right)^{-\frac{1}{2}} \left( \frac{R_{sph}^{max}}{10 \text{ km}} \right)^{\frac{3}{2}}. \quad (23)$$

This empirical formula involves only the mass  $M_{sph}^{max}$  and radius  $R_{sph}^{max}$  of the maximum mass nonrotating star for the given EOS. Haensel and Zdunik (1989) and Friedman *et al* (Friedman, Ipser, & Parker 1989) constructed this formula using realistic EOSs; it has an uncertainty of about 10 % (the Haensel-Zdunik coefficient is more accurate and has in these units the value 0.83). For a  $1.442 M_{\odot}$  maximum-mass nonrotating star Glendenning estimated the absolute minimum period to be 0.32-0.33 ms, which is 10-14 % larger than our computed value of 0.28 ms. The difference is as large as the uncertainty of the empirical formula (23), which is not surprising since (23) was constructed for a set of EOSs that is vastly different from the minimum-period EOSs. Our numerical results yield an empirical formula for the class of minimum-period EOSs which is fairly insensitive on the matching number density  $n_m$ . For a matching density of  $n_m = 0.1 \text{ fm}^{-3}$  the empirical formula is

$$\frac{P_{min}}{ms} = 0.740 \left( \frac{M_{sph}^{max}}{M_{\odot}} \right)^{-\frac{1}{2}} \left( \frac{R_{sph}^{max}}{10 \text{ km}} \right)^{\frac{3}{2}}, \quad (24)$$

with an approximate uncertainty of 0.3 %. This formula is accurate to about 1% for  $0.0 \leq n_m \leq 0.25 \text{ fm}^{-3}$ .

Rather than identifying a single class of minimum-period EOSs, Glendenning gave specific examples of minimum-period EOSs with and without a constant pressure region. As we have demonstrated, there is only

one class of minimum-period EOSs, and each EOS in the class has a constant pressure region. We believe that Glendenning missed this and proposed two classes of minimum period EOSs because he used a modified Levenberg-Marquardt method (Press et al. 1992) to minimize the function  $f(M, P) = w_1(M - M_{sph}^{max})^2 + w_2(P_{min})^2$ , where  $w_1$  and  $w_2$  are weights. Our own trials with this method showed that it is difficult simultaneously to obtain high accuracy for both  $M_{sph}^{max}$  and  $P_{min}$ .

## 8 ABSOLUTE MAXIMUM MASS OF UNIFORMLY ROTATING NEUTRON STARS

Among EOS satisfying assumptions (0-2) of section 2, that which yields a spherical model of maximum mass has a simple and unique form, consisting of two parts. The first part for low densities is a known low density EOS (earlier authors used the BPS (Baym, Pethick, & Sutherland 1971) and Negele-Vautherin EOS). The second part, for densities greater than some matching density  $\epsilon_m$ , is the causal limit EOS. Rhoades and Ruffini (1974) chose a particular  $\epsilon_m$  and computed a maximum mass of  $3.2 M_\odot$ . Although  $3.2 M_\odot$  continues to be quoted as the theoretical maximum mass for neutron stars,  $M_{max}$  is sensitive to the matching energy density  $\epsilon_m$  (as Hartle and Sabbadini (1977) pointed out) and a more accurate statement of the upper

limit set by causality on the mass of compact spherical stars is (Hartle 1978)

$$M_{sph}^{max} \simeq 4.8 \left( \frac{2 \times 10^{14} \text{ g/cm}^3}{\epsilon_m} \right)^{1/2} M_\odot. \quad (25)$$

This is in sharp contrast to the class of minimum-period EOSs, where due to the constant pressure region, the minimum period is insensitive to the matching density. So  $3.2 M_\odot$  corresponds to a specific choice of  $\epsilon_m$  and is not the theoretical maximum mass of neutron stars, which one needs to recompute whenever new certainty of the EOS allows one to increase the matching density.

Friedman and Ipser (1992) assumed that the EOS limited by causality yields the maximum mass for rotating stars as it does for nonrotating stars. They computed, using an independent code, the maximum mass for different matching densities, assuming the BPS or Negele-Vautherin EOS for low densities. We also computed the maximum mass of rotating compact stars using the FPS EOS and our numerical code, which is based on a different algorithm than the Friedman and Ipser code. Our results are summarized as

$$M_{rot}^{max} \simeq 6.1 \left( \frac{2 \times 10^{14} \text{ g/cm}^3}{\epsilon_m} \right)^{1/2} M_\odot, \quad (26)$$

which is 3 % larger than the Friedman and Ipser result, and is within the numerical accuracy of the code used by Friedman and Ipser. Using the FPS rather than the BPS EOS did not significantly affect the maximum mass. In (26),  $2 \times 10^{14} \text{ g/cm}^3$  is roughly the energy density up to which we trust the FPS EOS. If future research establishes the accuracy of FPS for higher

energy densities, then (26) can be used to give an updated, lower value for  $M_{rot}^{max}$ .

We acknowledge useful discussions with Bruce Allen, Lawrence Krauss, Lee Lindblom, and Tanmay Vachaspati. SK and NS acknowledge the support of NSF Grant Nos. 91-05935 and 95-07740 while at the University of Wisconsin-Milwaukee. SK acknowledges the support of Case Western Reserve University and the DOE.

## REFERENCES

Baym, G., Pethick, C., & Sutherland, P. 1971, ApJ, 170, 229

Cook, G. B., Shapiro, S. L., & Teukolsky, S. A. 1994, ApJ, 424, 823

Eriguchi, Y., Friedman, J. L., Gourgoulhon, E., Nozawa, T., & Stergioulas, N. 1996,  
in preparation

Friedman, J. L., & Ipser, J. R. 1987, ApJ, 314, 594

Friedman, J. L., & Ipser, J. R. 1992, Phil. Trans. R. Soc. Lond., A340, 391

Friedman, J. L., Ipser, J. R., & Parker, L. 1989, Phys. Rev. Lett., 62, 3015

Geroch, R., & Lindblom, L. 1991, Ann. Phys. 207, 394

Glendenning, N. K. 1992, Phys. Rev. D 46, 4161

Haensel, P., & Zdunik, J. L. 1989, Nature, 340, 617

Hartle, J. B. 1978, Phys. Repts., 46, 201

Hartle, J. B., & Sabbadini A. G. 1977, ApJ, 213, 831

Komatsu, H., Eriguchi, Y., & Hachisu, I. 1989, MNRAS, 239, 153

Pandharipande, V. R., & Ravenhall, D. G. 1989, in *Proceedings of the NATO Advanced Research Workshop on Nuclear Matter and Heavy Ion Collisions, Les Houches, 1989*, ed. M. Soyeur *et al.* (New York: Plenum), 103

Press, W. H., Flannery, B. P., Teukolsky, S. A., & Vetterling, W. T. 1992, Numerical Recipes in C, 2nd edition, (Cambridge: Cambridge Univ. Press)

Ravenhall, D. G. 1995, personal communication

Rhoades, C. E. Jr., & Ruffini R. 1974, Phys. Rev. Lett., 32, 324

Stergioulas, N., & Friedman, J. L. 1995, ApJ, 444, 306

Taylor, J. H., & Weisberg, J. M. 1989, ApJ, 345, 434

Figure 1: Schematic representations of the minimum-period EOSs (1) and (2). The minimum-period EOS (1) does not match a known low density EOS; the pressure vanishes for  $\epsilon < \epsilon_C$ , and is at the causal limit with  $dp/d\epsilon = 1$  for  $\epsilon > \epsilon_C$ . The minimum-period EOS (2) matches the FPS EOS to a constant pressure region at an energy density  $\epsilon_m$ . For  $\epsilon > \epsilon_C$  the EOS is at the causal limit with  $dp/d\epsilon = 1$ . Both axes are linear.

Figure 2: Minimum period EOSs (1) and (2) yielding a maximum-mass non-rotating star of  $M_{sph}^{max} = 1.442 M_{\odot}$ . The solid curve is the minimum period EOS (1), which does not match at low density to a known EOS. The energy density at which the EOS becomes causal is  $\epsilon_C = 2.156 \times 10^{15} g/cm^3$ . The central energy density of the minimum-period star is  $4.778 \times 10^{15} g/cm^3$  and is indicated by a filled circle on the solid curve. The dotted curve is the minimum-period EOS (2), which matches to the FPS EOS at low density. The energy density at which the EOS becomes causal is  $\epsilon_C = 2.157 \times 10^{15} g/cm^3$ . Above this density the EOSs are nearly identical and the solid curve overlaps the dashed curve. The central energy density of the minimum-period star is  $5.274 \times 10^{15} g/cm^3$  and is indicated by a filled triangle on the dotted curve. The matching number density is  $n_m = 0.1 fm^{-3}$ . Both axes are logarithmic.

Figure 3: The minimum period  $P_{min}$  allowed for a rotating, relativistic star as a function of the mass  $M_{sph}^{max}$  of the maximum-mass spherical star allowed by the EOS of the stellar matter. The upper curve is constructed using the minimum-period EOS (2), which matches at low density to the FPS EOS. The lower curve is constructed using the minimum-period EOS (1), which does not match at low density to a known low density EOS. Each curve divides the mass-period plane into two regions. The region below a curve is not accessible to stars with EOSs that satisfy the assumptions listed in section 2, and hence the region below the lower curve is not accessible to stars composed of matter obeying causality.

Figure 4: Minimum period  $P_{min}$  of rotating stars as a function of the allowed maximum mass  $M_{sph}^{max}$  of spherical stars for EOSs which are perturbations to the minimum-period EOS (2). The squares, triangles, and crosses represent EOSs obtained by different perturbations to the minimum period EOS, which are detailed in section 4.1. The solid curve represents the minimum-period EOS (2) and is the same as the upper curve in Figure 3. All of the points obtained from perturbed minimum-period EOSs lie above the solid curve.

Figure 5: Both plots show EOSs for different  $\kappa$  and  $\gamma$  using the parameterization (20) and (21). The  $\kappa\gamma$  parameterized EOS is fairly robust and can produce both stiff and soft EOSs. The bottom plot shows a sequence of EOSs, all of which yield  $M_{sph}^{max} = 1.442M_{\odot}$ . The period of the fastest rotating star decreases from left to right as the EOS approaches the minimum-period EOS (2). All axes are logarithmic.

Figure 6: Minimum period allowed by EOSs given by (20) and (21) for different values of the parameter  $\kappa$ . For given  $\kappa$ , the parameter  $\gamma$  is determined so that all EOSs sampled as one moves along the curve yield a maximum-mass nonrotating star with  $M_{sph}^{max} = 1.442 M_{\odot}$ . As  $\kappa \rightarrow 0$  the period tends asymptotically to its minimum value.

Figure 7: The minimum period  $P_{min}$  as a function of the mass  $M_{sph}^{max}$  of the maximum-mass spherical star, for different matching number densities  $n_m$ . From top to bottom the curves represent  $n_m = 0.5, 0.25, 0.1$ , and  $0.0 \text{ fm}^{-3}$ . Note that for  $n_m = 0.5 \text{ fm}^{-3}$  the maximum-mass spherical model cannot exceed  $2.38 M_\odot$ .

Figure 8: Mass vs. central energy density for sequences of models with constant angular momentum, constructed using the minimum-period EOS (1) with  $M_{sph}^{max} = 1.442 M_\odot$ . The solid curves are sequences of models with constant angular momentum, the bottom one corresponding to nonrotating models. The dashed curve is the sequence of models rotating at the Kepler limit while the dotted curve is the axisymmetric instability line defined by (22). The maximum-mass model is distinct from the model with maximum angular velocity  $\Omega_{max}$ . The period of the maximum-mass model is only 2% less than the period of the fastest rotating model.

Figure 1

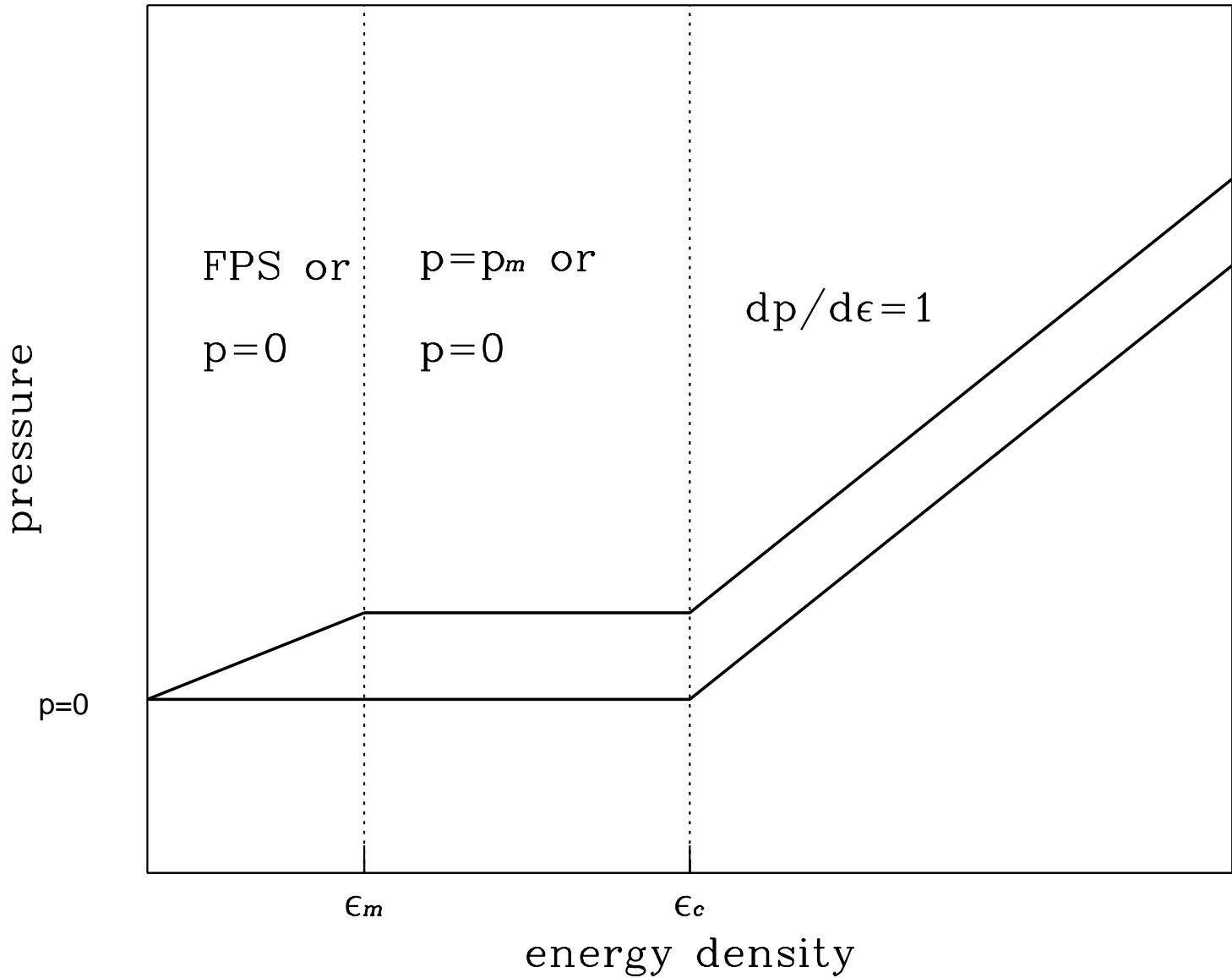


Figure 2

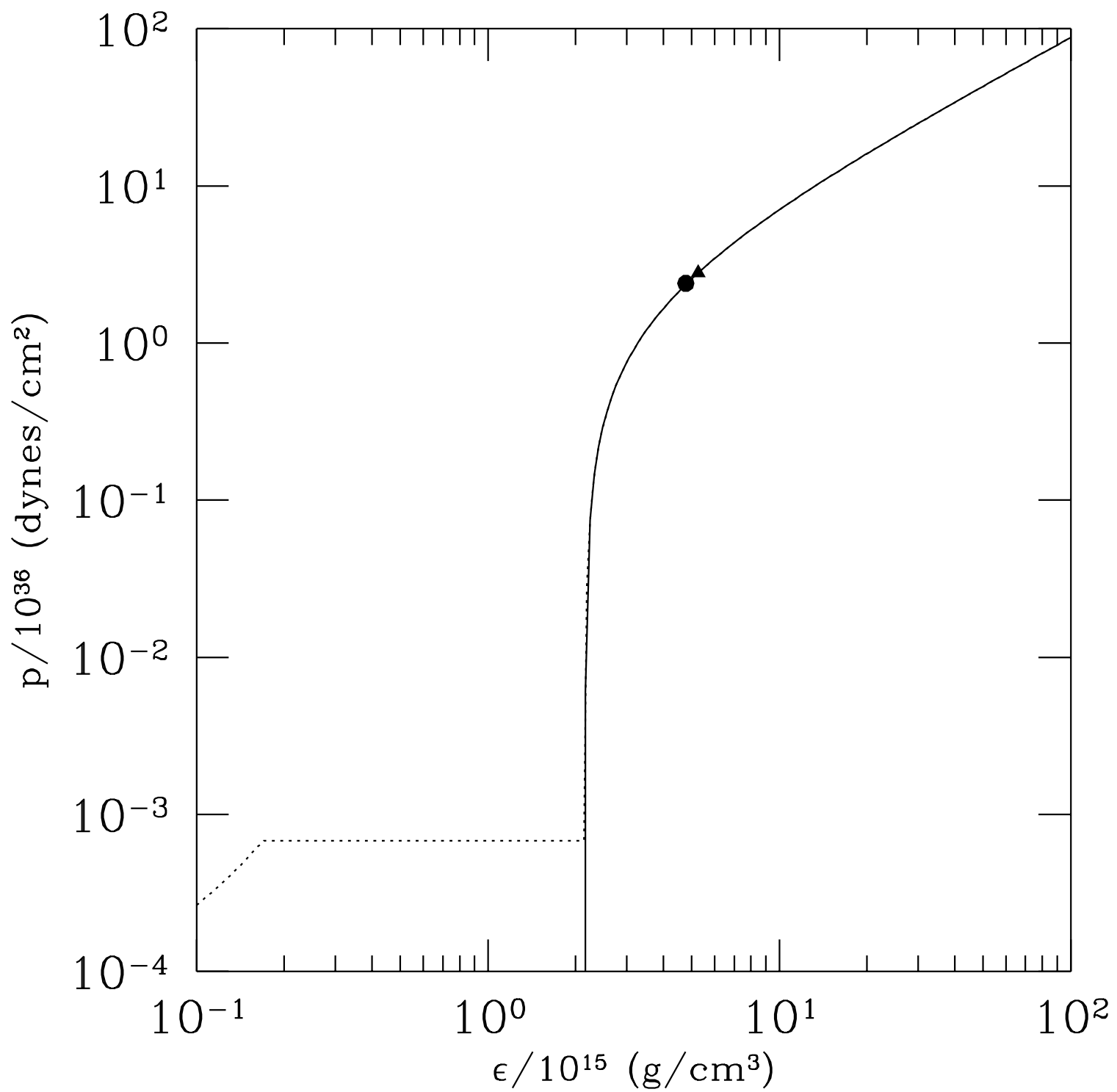


Figure 3

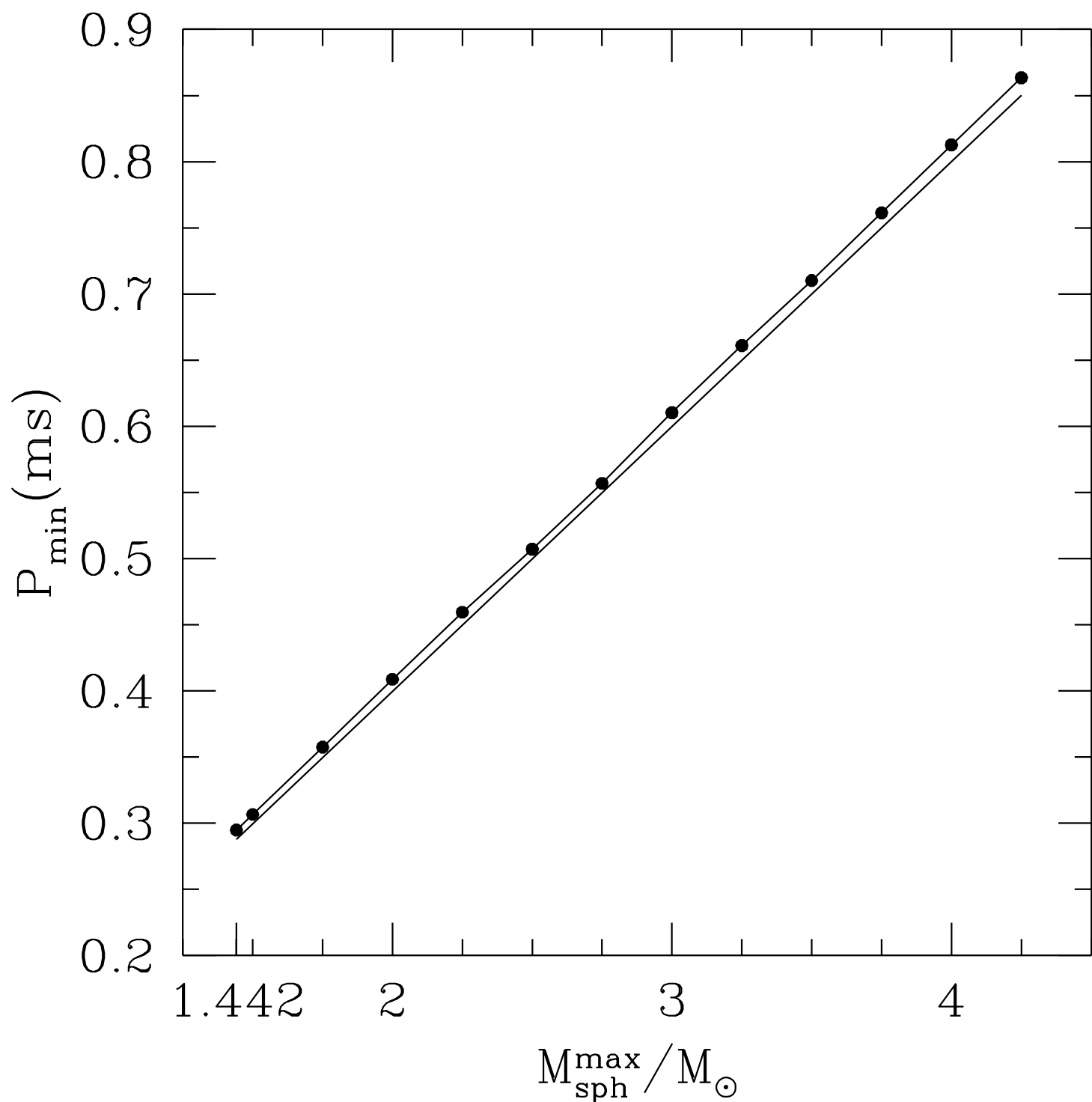


Figure 4

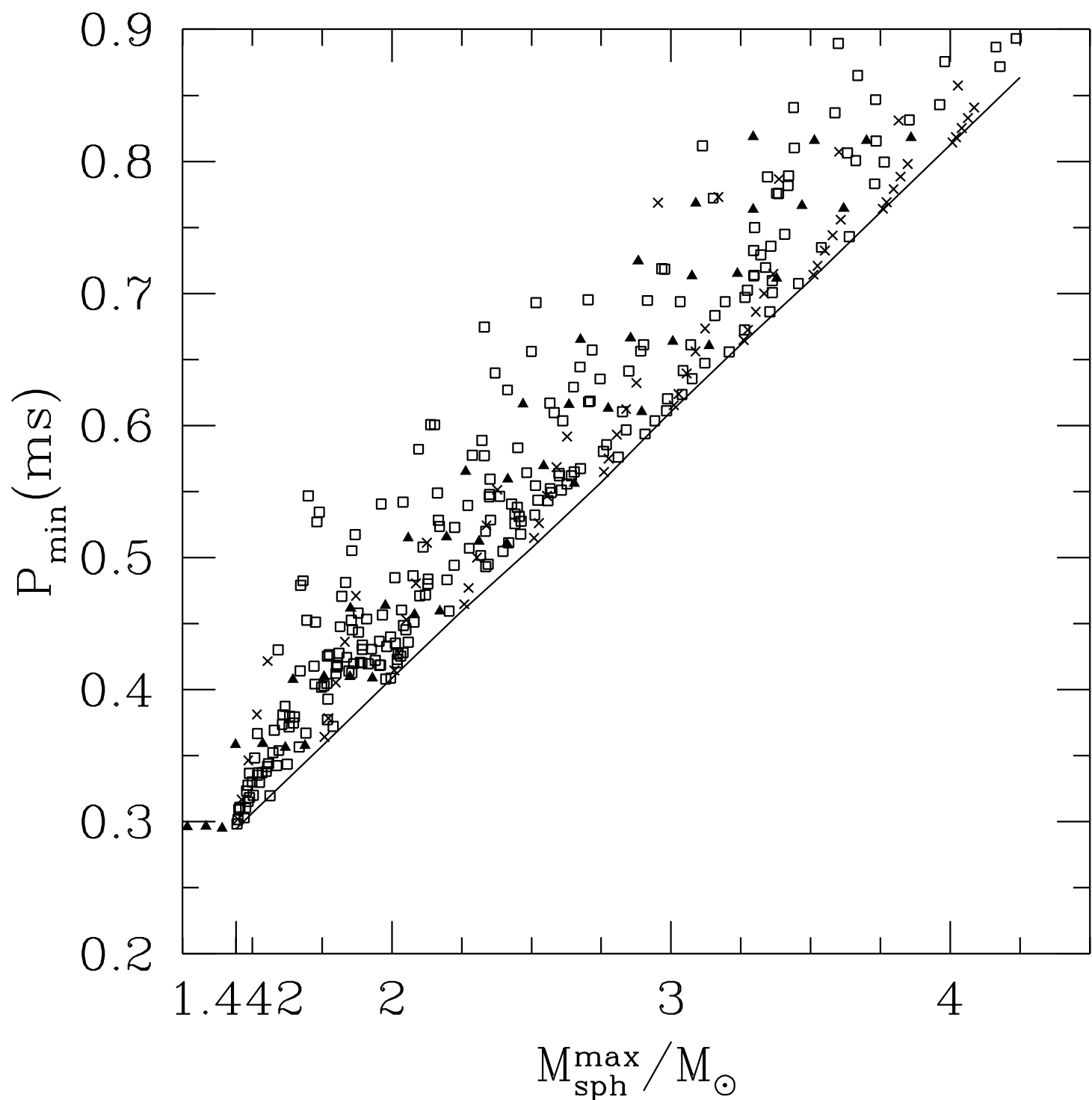


Figure 5

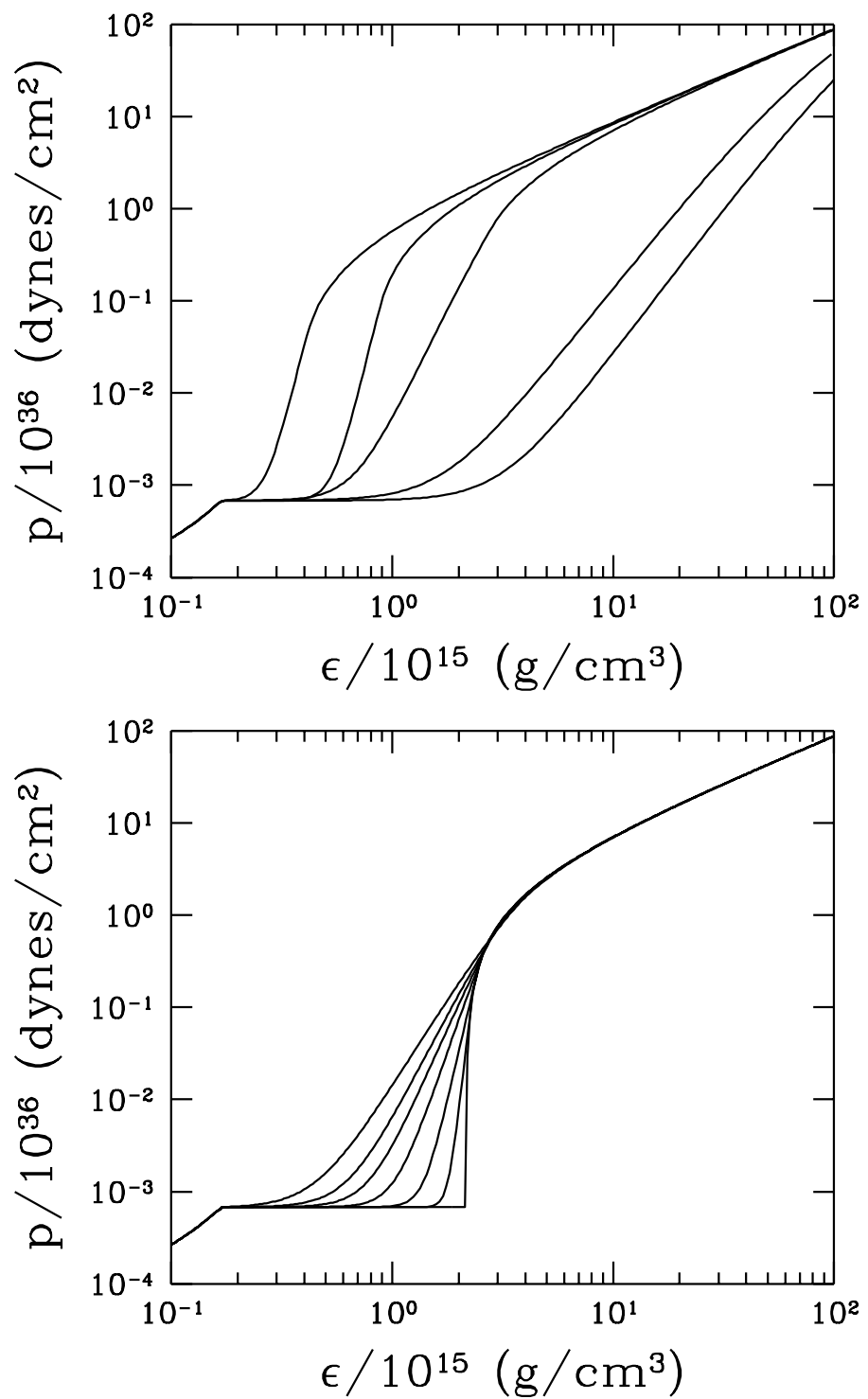


Figure 3

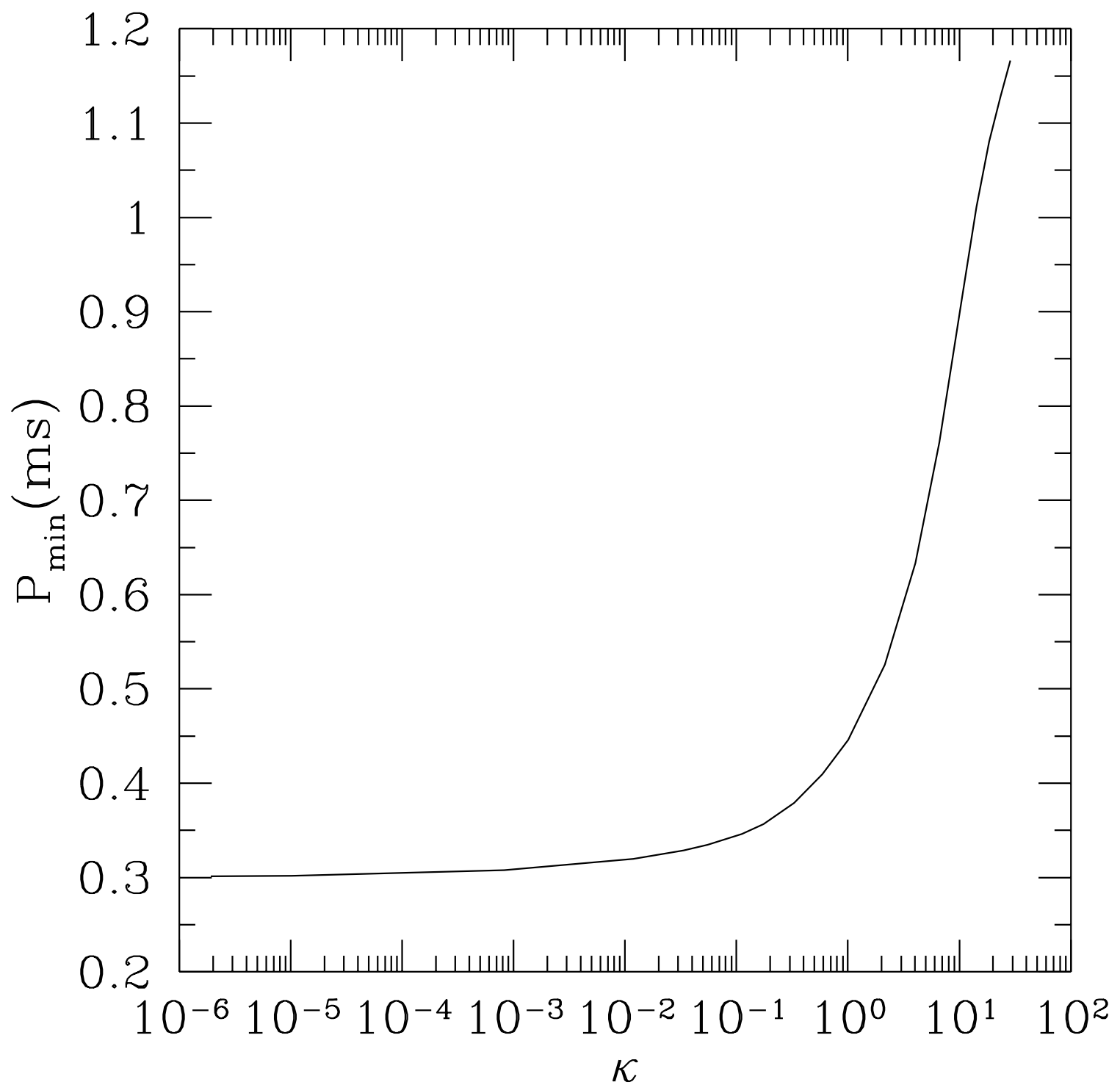


Figure 7

